RSC Advances

PAPER

View Article Online
View Journal | View Issue

Cite this: *RSC Adv.*, 2016, **6**, 68092

Highly efficient dye-sensitized solar cell performance from template derived high surface area mesoporous TiO_2 nanospheres

J. Archana,*[ab] S. Harish,[b] M. Sabarinathan,[b] M. Navaneethan,*[b] S. Ponnusamy,[a] C. Muthamizhchelvan,[a] M. Shimomura,[b] H. Ikeda,[b] D. K. Aswal[c] and Y. Hayakawa*[b]

Received 9th June 2016
Accepted 12th July 2016

DOI: 10.1039/c6ra14976f

www.rsc.org/advances

High surface area mesoporous anatase TiO_2 spheres are synthesized using ethylene glycol as a template by a solvothermal method. Electron microscopy studies revealed the formation of smooth surfaced mesoporous spheres with uniform size. A high surface area of 221.52 m^2 g^{-1} is obtained for the titanium tetraisopropoxide concentration of 0.5 mL. X-Ray diffraction and Raman analyses revealed the formation of anatase phase TiO_2. Uniform deposition of a mesoporous film for a photoanode was achieved by an optimized spray deposition method. The effects of the ruthenium dye-sensitizer N719 and indoline dye-sensitizer D205 on the dye sensitized solar cell performance are investigated. Maximum efficiencies of 8.96 and 9.02% are achieved using the sensitizers N719 and D205, respectively; from the mesoporous anatase TiO_2 sphere coated DSSC. IPCE analyses revealed that the mesoporous spheres efficiently collected the incident photons and achieved a conversion efficiency over 80% by internal reflections and a scattering process.

1. Introduction

Dye-sensitized solar cells (DSSCs) have attracted significant attention because of their potential in achieving efficient low-cost solar energy conversion, compared with silicon and group III–group V solar cells.[1–6] DSSCs typically consist of a fluorine-doped tin oxide (FTO) layer, photoanode, dye, electrolyte, and counter electrode.[7–10] Wide-band gap semiconductors such as ZnO and TiO_2 are well suited to and frequently used as photoanode materials. TiO_2 has a good affinity for organic molecules and a similar band alignment with common dyes. Therefore it is a preferred photoanode material over ZnO.[11–13] The highest reported DSSC energy conversion efficiency of 13% has been achieved using a TiO_2 nanoparticle film as the photo anode material.[14] Several factors are responsible for cell performance. Increasing the light harvesting efficiency will enhance the energy conversion efficiency. Semiconductor oxides with mesoporous structures have higher internal surface areas than the ones with nanocrystalline structures.[15–19]

Much effort has been made to modify the structure of photoanode materials. Sung Hoon *et al.*[20] prepared mesoporous TiO_2 films using graft co-polymers as a template, achieving a maximum efficiency of 4.6%. Satyanarayana Reddy *et al.*[21] used a soft template method for preparing mesoporous TiO_2 by employing various cationic surfactants as structure-directing and pore-forming agents. They achieved an efficiency of 7.5%. Hun-Gi Jung *et al.*[22] synthesized mesoporous TiO_2 spheres by a urea-assisted hydrothermal process. The resulting mesoporous TiO_2 electrode exhibited a higher efficiency (7.54%) than a commercial P25 TiO_2 electrode (5.69%). Xiaohuan *et al.*[23] had prepared mesoporous anatase TiO_2 microspheres by solvothermal process using phenol as a solvent. The average diameter of the synthesized spheres was 3 μm with the surface area of 168 m^2 g^{-1}. It yielded the conversion efficiency of 7.94%. Yuli Xiong[24] and his co-workers prepared highly ordered anatase 2D hexagonal mesoporous titania particles by ultrasonication method. Pluronic P123 was used as a surfactant template and HCl, H_2SO_4 as an acidic catalyst. It has the surface area of 121 m^2 g^{-1} and the device exhibited the efficiency of 4.93%. Jia-de-peng *et al.*[25] synthesized mesoporous TiO_2 spheres by hydrothermal method with an average diameter of 500 ± 60 nm with the surface area of 108.1 m^2 g^{-1}. The photoanode made of these spheres yielded the cell efficiency of 6.18%. Juti *et al.*[26] had synthesized the mesoporous anatase TiO_2 spheres by facile microwave assisted hydrothermal method. The average sizes of the spheres were around 800 nm with the surface area of 222 m^2 g^{-1}. The cell yielded the efficiency of 5.72%. Peter Chen *et al.*[27] prepared mesoporous anatase TiO_2 spheres by microwave

[a]*Department of Physics and Nanotechnology, SRM Research Institute, SRM University, Kattankulathur, Chennai, 603203, Tamil Nadu, India. E-mail: archana.jayaram@yahoo.com*

[b]*Research Institute of Electronics, Shizuoka University, 3-5-1 Johoku, Naka-Ku, Hamamatsu, Shizuoka 432-8011, Japan. E-mail: mpnavaneethan@yahoo.co.in; royhaya@ipc.shizuoka.ac.jp; Fax: +81-534781338; Tel: +81-534781338*

[c]*National Physical Laboratory, Dr K. S. Krishnan Marg, New Delhi – 110012, India*

assisted hydrothermal method. The size of the spheres was in the range of 400–600 nm with the surface area of 132.49 $m^2 g^{-1}$. The efficiency of the cell is 5.43%. Under the optimum condition with the scattering layer, the conversion efficiency was increased to 6.92%. Chang Soo *et al.*[28] prepared mesoporous anatase TiO_2 spheres by facile non hydrothermal method, synthesizing bulk calcinations process in which polymer ethyl cellulose were used a structure directing agent. Nanocrystalline layer exhibits the cell efficiency of 5.0%, when the mesoporous TiO_2 spheres were used as a scattering layer the efficiency was increased to 6.1%. Luo Tu *et al.*[29] fabricated the DSSC using mesoporous TiO_2 microspheres. The average size of the spheres was 1.1 μm with the surface area of 137 $m^2 g^{-1}$. The cell yielded the efficiency of 6.6%. Hui Tong[30] and his coworkers synthesized mesoporous TiO_2 microspheres by sol–gel method. The average diameter of the spheres was about 0.5 μm. They had investigated the surface area and pore size of the spheres without template (123 $m^2 g^{-1}$, 6.2 nm), with template Pluronic F127 as a template (148 $m^2 g^{-1}$, 5.4 nm) and TiO_2 aggregates (107 $m^2 g^{-1}$, 10.6 nm). TiO_2 aggregates with higher pore size gives good efficiency of 5.6% whereas the cell efficiency for without and with template were reported as 3.6% and 4.1%.

Photoanode materials consisting of mesoporous frameworks lead to good efficiencies. Their large surface area and interconnected network facilitate dye loading, charge transport, and light scattering.[31] Moreover, the high surface area with interconnected mesoporous TiO_2 spheres is required to obtain the high efficiency in DSSC. In this study, mesoporous anatase TiO_2 spheres with high surface area were solvothermally prepared using ethylene glycol as a templating agent. The effect of the titanium tetraisopropoxide (TTIP) precursor concentration on the formation and functional properties was investigated. The mesospheres were used to prepare photoanodes by spray deposition method. The effects of the sensitizers N719 and D205 on dye-sensitized solar cells performance were investigated.

2. Experimental method

2.1 Solvothermal growth of mesoporous TiO_2 spheres

All chemicals were purchased from Wako Chemicals (Japan) and were used without further purification. Two steps were typically followed to prepare the TiO_2 mesospheres.

2.1.1 Formation of titania glycolate spheres. Titanium tetraisopropoxide (0.5, 1.0, 1.5 and 2.0 mL) was added to ethylene glycol (50 mL). The solution was stirred for 5 h at room temperature, and then added to acetone bath (150 mL) containing trace water. The solution was stirred for 2 h to form a white suspension which was collected by centrifugation, thoroughly washed with distilled water and ethanol to remove impurities, and dried at 80 °C for 10 h. The samples were termed as S1 (0.5 mL), S2 (1.0 mL), S3 (1.5 mL) and S4 (2.0 mL), respectively.

2.1.2 Formation of mesoporous TiO_2 spheres. The titania glycolate spheres were dispersed in an equal volume of water and ethanol (30 mL), and stirred for 2 h. The white solution was transferred to a 100 mL Teflon-lined stainless steel autoclave, and heated at 150 °C for 12 h. The resulting product was collected and annealed at 300 °C for 2 h.

2.2 Characterization

Surface morphologies were observed by field-emission scanning electron microscopy (FESEM) with a JEOL JSM 7001F microscope. Transmission electron microscopy (TEM) images were recorded using a JEOL JEM 2100F microscope at an accelerating voltage of 200 kV. Crystalline phases were determined by X-ray diffraction (XRD), using a Rigaku diffractometer (RINT-2200, Japan, CuK_α radiation) with a 0.02° s^{-1} scan rate. Raman spectra were obtained using a JASCO NR-1800 spectrometer. Ultraviolet-visible (UV-vis) absorption spectra were measured using a Shimadzu 3100 PC spectrophotometer (Japan). Fourier transform infrared (FTIR) spectra were recorded using a JASCO MFT 2000 spectrometer from KBr pellet samples. Current density and voltage (*I–V*) characteristics were measured at an air mass of AM 1.5 (100 mW cm^{-2} of simulated sunlight) by a JASCO solar simulator equipped with a Keithley picoammeter. Impedance analysis was performed using Solartron (model no. 1280C) Electrochemical Test System.

2.3 Dye-sensitized solar cell fabrication

The fabrication procedure was adopted from our previous report.[31] Mesoporous TiO_2 powder was dispersed in ethanol, and ground for 30 min using an ultrasonic processor. Five drops of triton-X were added to the solution as a binder. The solution was sprayed on FTO glass (Nippon Sheet Glass, 8.7 Ω $sq.^{-1}$, 80% transparency in the visible range) at 150 °C by spray pyrolysis. The TiO_2 films were annealed at 450 °C for 2 h. The resulting photoanodes were soaked in an ethanol solution containing 0.03 M ditetrabutylammonium *cis*-bis(isothiocyanato)bis(2,2″-bipyridyl-4,4′-dicarboxylato)ruthenium(II) (N719) for 12 h. The photoanode was clamped with a Pt-coated FTO counter electrode to form a sandwich-type cell. A redox electrolyte solution was filled between the electrodes by capillary action to form the cell. The electrolyte consisted of 0.6 M dimethylpropylimidazolium iodide, 0.1 M lithium iodide, 0.01 M iodine, and 0.5 M tetrabutylpyridine in acetonitrile (FUNCHEM, Tomiyama electrolyte company, Japan).

3. Results and discussion

Fig. 1–4 show FESEM and TEM images of the titania glycolate and TiO_2 spheres. The TTIP concentrations used in the preparations were 0.5, 1.0, 1.5 and 2.0 mL for Fig. 1–4, respectively. Fig. 1–4(a) show typical FESEM images of the titania glycolate spheres, which exhibited an average size of 100–200 nm and very smooth surfaces. Porous TiO_2 spheres were formed after solvothermal treatment, as shown in Fig. 1–4(b). TEM images of the porous TiO_2 spheres are shown in Fig. 1–4(c). The formation of the spherical structure depended on the precursor concentration. When the TTIP concentration was 0.5 mL, the resulting TiO_2 spheres exhibited good interconnectivity and defined boundaries as shown in Fig. 1(c). As the TTIP concentration increased to 1.0, 1.5 and 2.0 mL, the morphology of the products became progressively more irregular. Defined boundaries

were not observed in Fig. 2(c). High-magnification TEM images of products prepared from TTIP concentrations of 0.5, 1.0, 1.5 and 2.0 mL are shown in Fig. 1–4(d), respectively. High-resolution TEM (HRTEM) images are shown inset. The prepared materials exhibited good crystallinity with an average particle size of 5–8 nm. Thus, the TiO_2 mesosphere morphology could be tuned by the concentration of the TTIP precursor.

Brunauer–Emmett–Teller (BET) analysis was performed to determine the surface area of the TiO_2 spheres, and to better understand their mesoporous frameworks.[33] Fig. 5(a) shows N_2 adsorption–desorption isotherms and pore size distributions estimated using the Barrett–Joyner–Halenda (BJH) analysis. Fig. 5(b) shows that all isotherms exhibited type IV behavior with H1 hysteresis loops, which is characteristic of mesoporous structures. The surface area of the samples prepared from various TTIP concentrations were determined from BET analysis. A TTIP concentration of 0.5 mL resulted in a surface area of 221.52 $m^2\ g^{-1}$. TTIP concentrations of 1.0, 1.5 and 2.0 mL resulted in surface areas of 169.60, 166.52 and 133.68 $m^2\ g^{-1}$, respectively. Thus, an increasing TTIP concentration resulted in decreased BET surface areas. This was in good agreement with the TEM results, which showed a similar trend.

The formation process of the mesoporous TiO_2 is shown in Fig. 5(c). Titanium metal oxides contain moisture-sensitive alkoxide groups, so TTIP tends to hydrolyze during titania synthesis. A high hydrolysis rate leads to non-uniform products, so it is necessary to slow this process. Branched alkoxy ligands sterically suppress hydrolysis, so ethylene glycol was chosen to suppress hydrolysis by the nucleophilic substitution mechanism. The alkyl chain of ethylene glycol coordinates with TiO_2 nuclei to form titania glycolate,[32] according to:

$$Ti(OiPr)_4 + 2HO(CH_2)_2OH \rightarrow Ti((OCH_2)_2)_2 + 4iPrOH \quad (1)$$

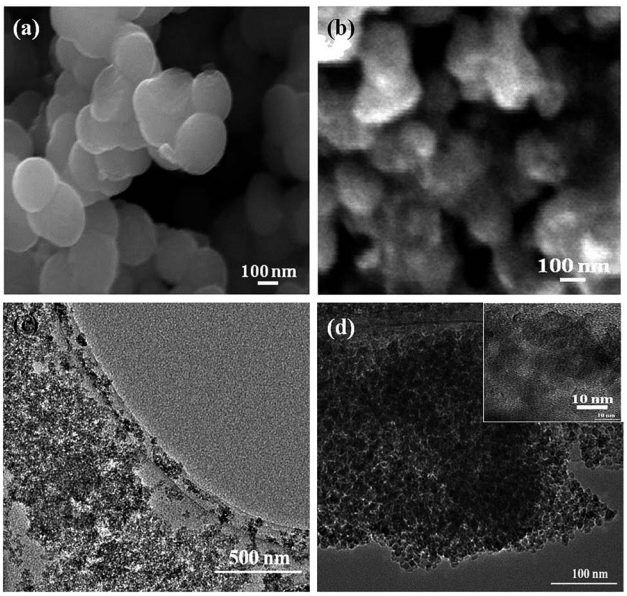

Fig. 2 FESEM images of (a) titania glycolate spheres and (b) mesoporous TiO_2 spheres, (c)–(d) TEM images of mesoporous TiO_2 spheres (inset shows a HRTEM image) of S2.

Titania glycolate was treated with acetone to enhance the hydrolysis of the glycolate precursor, and a solvothermal process was employed to synthesis the mesoporous anatase TiO_2 spheres. During this process, coordination between the alkyl chain of ethylene glycolate and titania was broken. Releasing the alkoxy group from the product resulted in the mesoporous TiO_2. TEM indicated that the increased TTIP concentration affected the structure of the TiO_2 spheres. The number of TiO_2 nuclei was proportional to the number of alkoxy

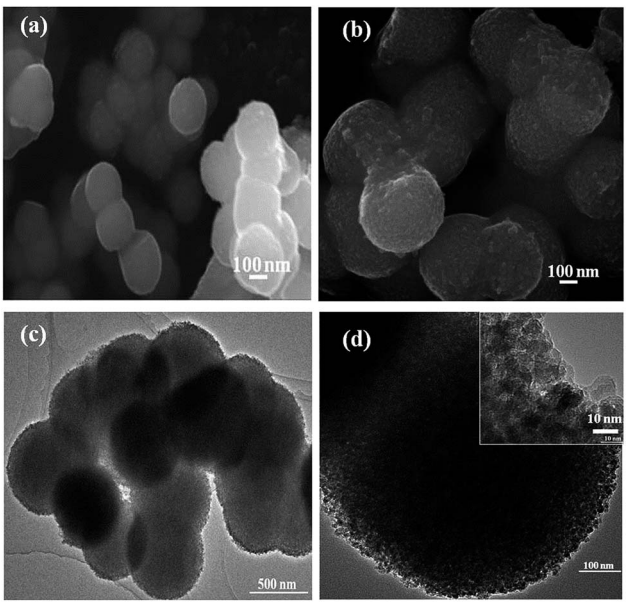

Fig. 1 FESEM images of (a) titania glycolate spheres and (b) mesoporous TiO_2 spheres, (c)–(d) TEM images of mesoporous TiO_2 spheres (inset shows a HRTEM image) of S1.

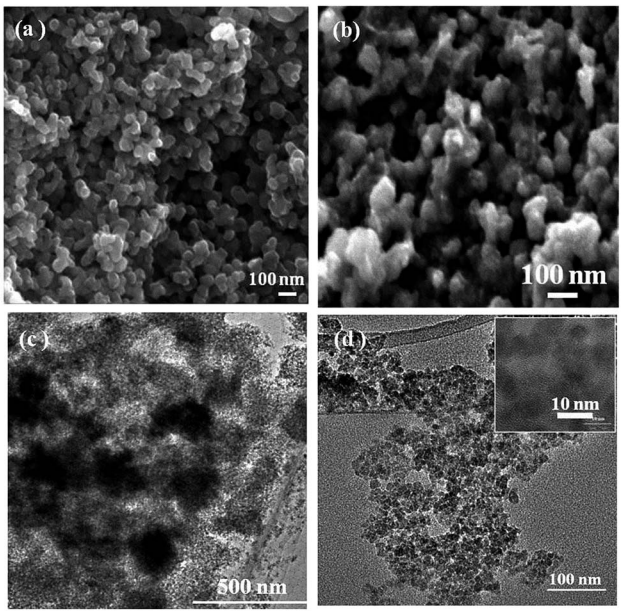

Fig. 3 FESEM images of (a) titania glycolate spheres and (b) mesoporous TiO_2 spheres, (c)–(d) TEM images of mesoporous TiO_2 spheres (inset shows a HRTEM image) of S3.

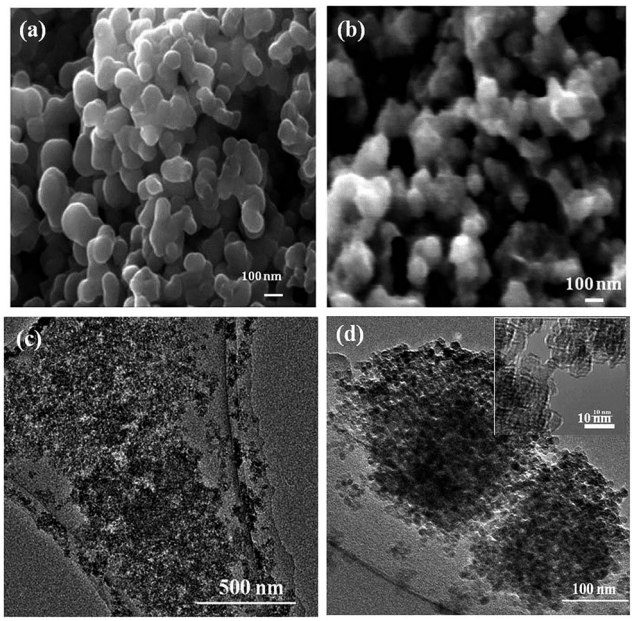

Fig. 4 FESEM images of (a) titania glycolate spheres and (b) mesoporous TiO_2 spheres. (c)–(d) TEM images of mesoporous TiO_2 spheres (inset shows a HRTEM image) of S4.

groups released from ethylene glycol. Increasing the TTIP concentration from 0.5 to 2.0 mL increased the number of TiO_2 nuclei in solution. The alkyl chain content of ethylene glycol is constant, so the resulting imbalance in coordination bonds was responsible for the formation of the different surface morphology. Thus, the TTIP concentration played an important role in determining the particle morphology. 0.5 mL of TTIP evidently provided favorable coordination between TiO_2 nuclei and alkyl chains, because defined interconnected structures were observed when comparing with higher TTIP concentration products.

Fig. 6(a) shows XRD patterns of the samples. Peaks at 25.19, 37.8, 48.1, 53.5, 55.1, 62.3, 70.2 and 75.2° corresponded to reflections from the (101), (004), (200), (105), (204), (220) and (215) crystal planes, respectively. All these diffraction peaks were assigned to anatase TiO_2 (JCPDS card no. 21-1272). No peaks related to other phases such as rutile and brookite were observed. The broadening of the diffraction peaks indicated that the TiO_2 mesoporous spheres were composed of smaller particles. Fig. 6(b) shows the Raman spectrum of the mesoporous TiO_2 spheres. According to factor group theory, anatase TiO_2 has six Raman active modes ($A_{1g} + 2B_{1g} + 3E_g$). Oshaka *et al.* reported that these six allowed bands were consistent with the first-order Raman spectrum.[34] These bands were observed at 144 (E_g), 197 (Eg), 399 (B_{1g}), 513 (A_{1g}), 519 (B_{1g}) and 639 (E_g) cm^{-1}.[35,36] In the current study, Raman bands of the TiO_2 mesospheres at 148, 400, 518, and 640 cm^{-1} corresponded to the anatase phase. The observed bands were in agreement with the bands of anatase TiO_2. The E_g and B_{1g} bands were shifted to a slightly higher wavenumber. Choi *et al.* attributed this shift to two main factors. The first was a contraction of nanoparticle volume caused by

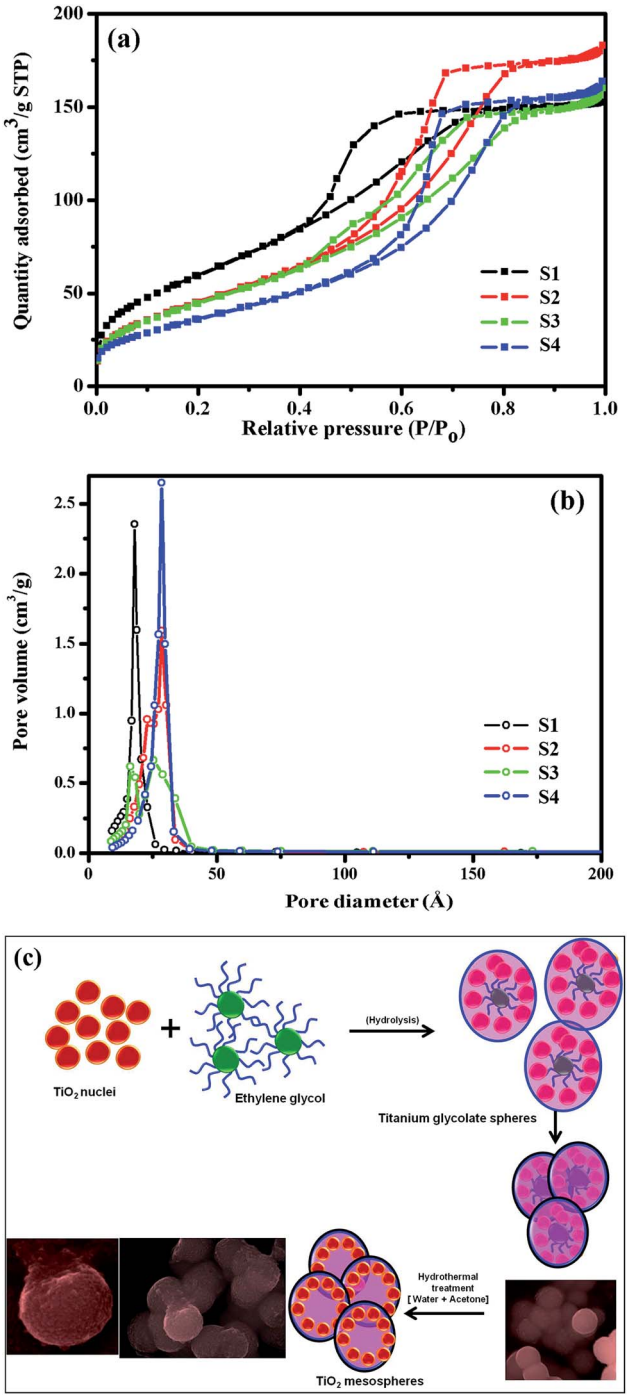

Fig. 5 (a) N_2 sorption isotherms and (b) BJH pore size distribution of the mesoporous TiO_2 spheres and (c) schematic formation mechanism of the mesoporous TiO_2 spheres.

the radial pressure, which tends to increase the force constant (k). The second was the effect of contraction, which decreases the vibrational amplitude of associating neighbor bonds, because of increased static disorder.[37] The shift in Raman peaks occurred because of the decrease in particle size, because the TiO_2 sample consisted of small particles as shown by HRTEM.

Fig. 6(c) shows UV-vis absorption spectra of the samples. All samples exhibited a significant absorption onset at wavelength less than 400 nm. This is attributed to the intrinsic band gap absorption of TiO_2. An optical absorption onset in the visible region was expected, because the mesospheres possess significant light scattering capability. The TiO_2 mesospheres facilitated visible photon absorption by the dye, and enhanced light harvesting during DSSC performance. TiO_2 mesospheres (0.5 mL of TTIP) exhibited higher absorbance compared to other samples which indicated that it possessed excellent optical properties.

The obtained TiO_2 mesospheres coated photoanode (0.5 mL TTIP) was cleaved to identify the nature of the deposition, interface of FTO:TiO_2 mesospheres and morphology of TiO_2 mesospheres. Fig. 7(a) and (b) shows the FESEM images of cross-section and top views of photoanode, respectively. The TiO_2 mesospheres were well-deposited on the FTO layers and possessed the mesoporous sphere morphology as shown in the inset of the figure. Top view of the photoanode revealed that the TiO_2 mesospheres were deposited uniformly without any cracks and the good interconnectivity of the mesospheres which enhances the dye adsorption and electron transport.

Fig. 7(c) shows *I–V* curves of N719 sensitized DSSCs. Their photovoltaic parameters are summarized in Table 1. The DSSC containing the electrode fabricated with TiO_2 mesospheres (0.5 mL of TTIP) exhibited a high energy conversion efficiency of 8.96%, because of its higher J_{sc} value of 19.09 mA cm^{-2}. The DSSCs containing electrodes prepared with 1.0, 1.5 and 2.0 mL of TTIP exhibited gradually decreasing J_{sc} values of 17.72, 14.77 and 12.32 mA cm^{-2}, yielding efficiencies of 8.43, 7.22 and 6.05%, respectively. Moreover, amount of the dye adsorptions on the photoanodes were obtained using the UV visible absorption

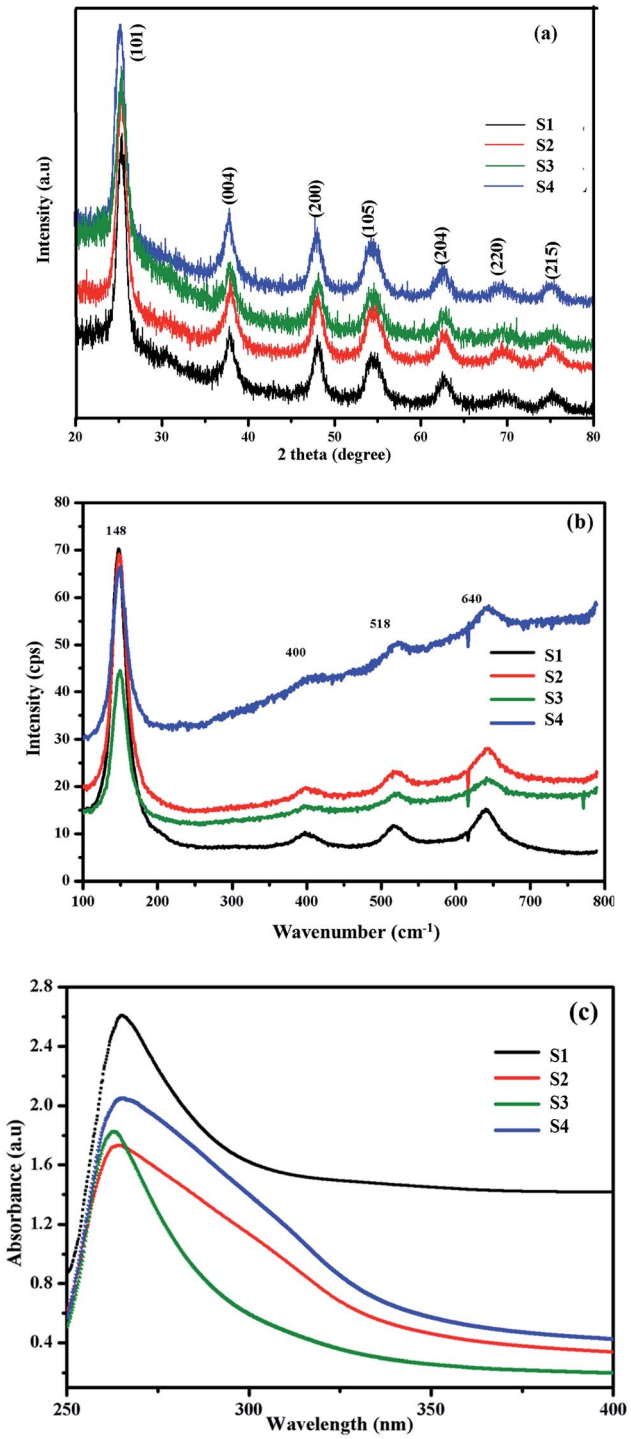

Fig. 6 (a) XRD patterns, (b) Raman spectra and (c) optical absorption spectra of the mesoporous TiO_2 spheres.

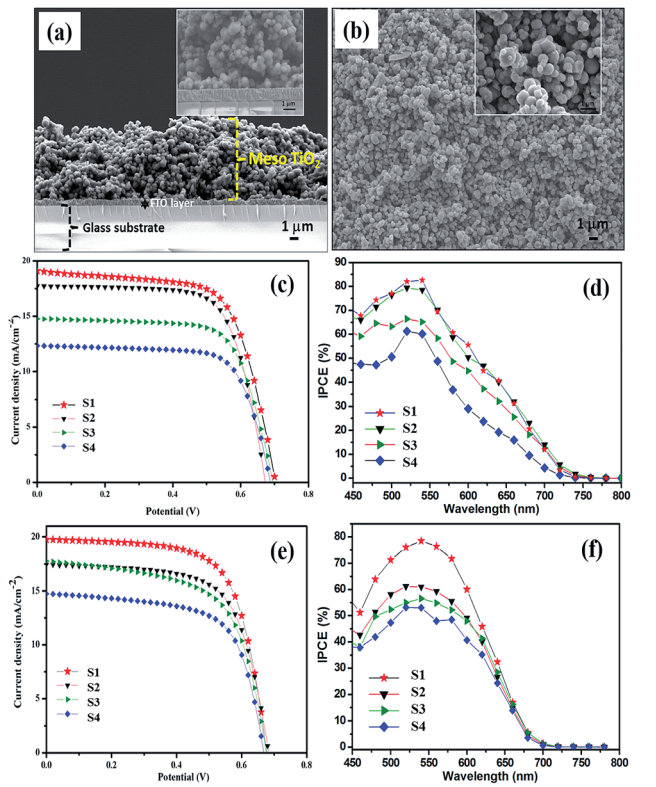

Fig. 7 FESEM images of (a) cross-section, (b) top views of mesoporous TiO_2 spheres (0.5 mL TTIP) coated photoanode (inset: magnified regions), (c) *J–V* (N719 dye), (d) IPCE characteristic curves of DSSCs (N719 dye), (e) *J–V* (D205 dye) and (f) IPCE characteristics of DSSCs (D205 dye).

Table 1 Photovoltaic performance of DSSCs prepared using mesoporous TiO_2 spheres sensitized by N719 dye at AM 1.5 (100 mW cm^{-2})

Device	S1	S2	S3	S4
Thickness (μm)	16 ± 0.5	16 ± 0.5	16 ± 0.5	16 ± 0.5
FF	0.66	0.70	0.70	0.71
V_{oc} (V)	0.70	0.67	0.69	0.68
J_{sc} (mA cm^{-2})	19.09	17.72	14.77	12.32
EFF (%)	8.96	8.43	7.22	6.05
Amount of adsorbed dye (10^{-7} mol cm^{-2})	1.95	1.68	1.33	1.07
BET surface area (m^2 g^{-1})	221.52	169.60	166.52	133.68
IPCE (%)	83.13	79.68	66.87	61.68
R_p (Ω)	3.2	9.2	64.4	148.8

spectrometer by soaking dye-sensitized photoanodes in 1 M NaOH solution. The obtained results are tabulated in Table 1. The TiO_2 mesospheres (0.5 mL of TTIP) coated dye-sensitized photoanodes exhibited a value of 1.95 × 10^{-7} mol cm^{-2} and this is higher than that of other photoanodes. From the above results, it is evident that the TiO_2 mesospheres (0.5 mL of TTIP) has high surface area, well-defined interconnected mesoporous network and high dye-adsorption and thus facilitated the high efficiency compared to other samples such as 1.0, 1.5 and 2 mL concentration of TTIP.

The incident photon to current conversion efficiency (IPCE) provide further evidence for the excellent electron transport property of mesoporous TiO_2. Fig. 7(d) shows the IPCE spectra of N719 dye sensitized device prepared using 0.5, 1.0, 1.5 and 2.0 mL of TTIP as photoanode material. The wavelength of N719 sensitized devices is usually observed at a wavelength of 530–550 nm, the IPCE values is observed as 83.13% for 0.5 mL. The increase in the concentration of TTIP to 1.0, 1.5 and 2.0 mL led to the decrease in IPCE value to 79.68, 66.87 and 61.68%. The steady decrease in IPCE value is attributed to the decrease in I_{sc} by increased concentration of TTIP.[38,39] The improved in IPCE performance was due to enhanced charge generation efficiency, inhibition of electron recombination and high dye loading.[40,41]

Metal-free D205 was also used as a sensitizer, in place of the Ru-containing N719 dye, and the performances of the resulting devices were studied. Fig. 7(e) shows the *I–V* curves of the D205-sensitized devices and the parameters are tabulated in Table 2. Similarly to the results for the N719-sensitized DSSCs, a higher energy conversion efficiency was obtained for the TiO_2 mesospheres (0.5 mL of TTIP) coated DSSC. The conversion and

Table 2 Photovoltaic performance of DSSCs prepared using mesoporous TiO_2 spheres sensitized by D205 dye at AM 1.5 (100 mW cm^{-2})

Device	S1	S2	S3	S4
Thickness (μm)	16 ± 0.5	16 ± 0.5	16 ± 0.5	16 ± 0.5
FF	0.67	0.66	0.61	0.65
V_{oc} (V)	0.67	0.68	0.67	0.68
J_{sc} (mA cm^{-2})	19.74	17.40	17.77	14.74
EFF (%)	9.02	7.92	7.43	6.44
IPCE (%)	78.70	61.67	57.26	53.71
R_p (Ω)	3.0	6.0	60.5	120.8

J_{sc} were 9.02% and 19.74 mA cm^{-2}, respectively. The J_{sc} values were 17.77, 17.40 and 14.74 mA cm^{-2}, and the efficiencies were 7.92, 7.43 and 6.44% for the DSSCs prepared from 1.0, 1.5 and 2.0 mL of TTIP, respectively. The highest efficiencies of 8.96% for N719 and 9.02% for D205 were obtained when 0.5 mL of TTIP was used to prepare the TiO_2 mesospheres. 0.5 mL TTIP concentration resulted in good interconnectivity and defined boundaries, which enhanced dye adsorption and facilitated electron transport, compared with the other TTIP concentrations. Fig. 7(f) shows the incident photon to current conversion efficiency (IPCE) measured was performed on the mesoporous TiO_2. D205 sensitized device has a broad absorption peak covering almost the entire visible spectra from 450–600 nm, the IPCE values is observed as 78.70% for 0.5 mL. With further increase in the concentration of TTIP to 1.0, 1.5 and 2.0 mL led to the decrease in IPCE value to 61.67, 57.26 and 53.71%. To understand the interfacial charge transfer and the recombination process the electrochemical impedance spectra (EIS) were taken in the range of (0–20 kHz). Fig. 8(a) and (b) shows the EIS spectra of the device sensitized by N719 and D205 dye sensitizers, respectively. The charge transfer resistance of the semiconductor electrolyte interface (R_p) can be calculated from the

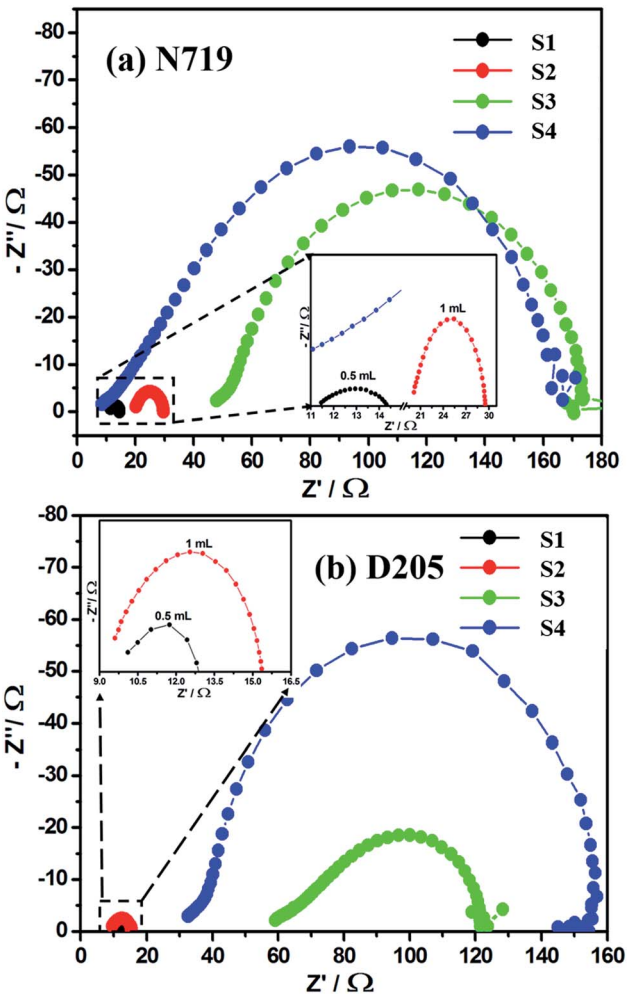

Fig. 8 EIS spectra of DSSCs prepared using the mesoporous TiO_2 spheres sensitized by (a) N719 and (b) D205 dyes.

semicircles of the spectrua. Accordingly the device using N719 as a sensitizer, the R_p value is observed as 3.2 Ω for 0.5 mL. Whereas, it increases with higher concentration as 9.2 Ω (1.0 mL), 64.4 Ω (1.5 mL) and 148.8 Ω (2.0 mL). Similarly, in the case of D205 it is noted as 3.0 Ω for 0.5 mL and 6.0 Ω (1.0 mL), 60.5 Ω (1.5 mL) and 120.8 Ω (2.0 mL). In general, the decrease in the R_p value represents the enhancement in the dye adsorption.[42,43] Thus it is worthy to note in both the cases of N719 and D205 as sensitizers the R_p value is lower for the 0.5 mL. It has the good agreement with the TEM and *I–V* measurements.

4. Conclusions

High surface area mesoporous anatase TiO_2 nanospheres were synthesized by solvothermal growth using ethylene glycol as a template. The effect of the precursor TTIP concentration on the morphology, structure, and optical properties of the mesoporous TiO_2 nanospheres was investigated. TiO_2 nanospheres were characterized by FESEM, TEM, N_2 sorption measurements, XRD, Raman spectroscopy and UV-vis absorption spectrophotometry. A TTIP concentration of 0.5 mL resulted in excellent interparticle connection with well-defined boundaries, compared with higher TTIP concentrations (1.0, 1.5 and 2.0 mL). The TiO_2 mesospheres were used to prepare photoanodes, and the performances of the resulting DSSCs were studied. The effect of the sensitizers N719 and D205 on device performance was investigated. A maximum efficiency of 8.96% was achieved when using N719, and that of 9.02% was achieved when using D205, at a TTIP concentration of 0.5 mL for a thickness of 16 μm.

Acknowledgements

This work was financially supported by Grant-in-Aid for Scientific Research (B) (25289087), Grant-in-Aid for JSPS Fellows (24-12363, 25-13360) from the Ministry of Education, Culture, Sports, Science and Technology of Japan, and the cooperative research projects of the Research Institute of Electronics, Shizuoka University. The authors would like to thank Center for Instrumental Analysis, Shizuoka University, Hamamatsu, Japan for the characterization techniques. We thank Prof. K. Murakami, Prof. Masayuki Okuya for *I–V* and IPCE measurements. J. Archana would like to thank JSPS, Japan, for their award of JSPS research fellowship.

References

1 B. O'Regan and M. Gratzel, *Nature*, 1991, **353**, 737–740.
2 J. Lin, L. Zhao, Y.-U. Heo, L. Wang, F. H. Bijarbooneh, A. J. Mozer, A. Nattestad, Y. Yamauchi, S. X. Dou and J. H. Kim, *Nano Energy*, 2015, **11**, 557–567.
3 J. Lin, Y.-U. Heo, A. Nattestad, Y. Yamauchi, S. X. Dou and J. H. Kim, *Electrochim. Acta*, 2015, **153**, 393–398.
4 H. J. Snaith, *Adv. Funct. Mater.*, 2010, **20**, 13–19.
5 G. J. Meyer, *ACS Nano*, 2010, **4**, 4337–4343.
6 M. Gratzel, *Inorg. Chem.*, 2005, **44**, 6841–6851.
7 T. Yamaguchi, N. Tobe, D. Matsumoto, T. Nagai and H. Arakawa, *Sol. Energy Mater. Sol. Cells*, 2010, **94**, 812–816.
8 J. Kim, J. K. Koh, B. Kim, J. H. Kim and E. Kim, *Angew. Chem., Int. Ed.*, 2012, **51**, 6864–6869.
9 I. Robel, V. Subramanian, M. Kuno and P. V. Kamat, *J. Am. Chem. Soc.*, 2006, **128**, 2385–2393.
10 J. K. Koh, J. Kim, B. Kim, J. H. Kim and E. Kim, *Adv. Mater.*, 2011, **23**, 1641–1646.
11 Y. Saito, S. Kambe, T. Kitamura, Y. Wada and S. Yanagida, *Sol. Energy Mater. Sol. Cells*, 2004, **83**, 1–13.
12 M. Y. Song, D. K. Kim, K. J. Ihn, S. M. Jo and D. Y. Kim, *Nanotechnology*, 2004, **15**, 1861–1865.
13 H. G. Jung, C. S. Yoon, J. Prakash and Y. K. Sun, *J. Phys. Chem. C*, 2009, **113**, 21258–21263.
14 C. Yasuo, I. Ashraful, W. Yuki, K. Ryoichi, K. Naoki and H. Liyuan, *Jpn. J. Appl. Phys.*, 2006, **45**, 638–640.
15 Y. Wang, X. Tang, L. Yin, W. Huang, Y. R. Hacohen and A. Gedanken, *Adv. Mater.*, 2000, **12**, 1183–1186.
16 P. Kluson, P. Kacer, T. Cajthaml and M. Kalaji, *J. Mater. Chem.*, 2001, **11**, 644–651.
17 M. Gratzel, *Curr. Opin. Colloid Interface Sci.*, 1999, **4**, 314–321.
18 X. Lu, G. Li and J. C. Yu, *Langmuir*, 2010, **26**, 3031–3039.
19 S. Liu, J. Yu and C. Jaronie, *J. Am. Chem. Soc.*, 2010, **132**, 11914–11916.
20 A. Sung Hoon, K. Joo Hwan, S. Jin Ah and K. Jong Hak, *Chem. Commun.*, 2010, **46**, 1935–1937.
21 G. Satyanarayana Reddy, A. Krishnamoorthy, Y. Chrisotpher, M. Gratzel and B. Palani, *Energy Environ. Sci.*, 2010, **3**, 838–845.
22 J. Hun Gi, K. Yong Soo and S. Yang kook, *Electrochim. Acta*, 2010, **55**, 4637–4641.
23 M. Xiaohuan, P. Kai, P. L. Yong, Z. Wei, P. Qingjiang, T. Guohui and W. GuoFeng, *J. Mater. Chem. A*, 2013, **1**, 9853–9861.
24 Y. Xiong, D. He, Y. Jin, P. J. Cameron and K. J. Edler, *J. Phys. Chem. C*, 2015, **119**, 22552–22559.
25 J. D. Peng, C. P. Lee, D. Velayutham, V. Suryanarayanan and K. C. Ho, *J. Mater. Chem. A*, 2015, **3**, 6383–6391.
26 J. R. Deka and H. W. Wang, *J. Chin. Chem. Soc.*, 2014, **61**, 1049–1055.
27 P. Chen, J. D. Peng, C. H. Liao, P. S. Shen and P. L. Kuo, *J. Nanopart. Res.*, 2013, **15**, 1465–1476.
28 S. L. Chang, Y. L. Jung, S. C. Won and H. K. Jong, *Electrochim. Acta*, 2015, **173**, 139–147.
29 T. Luo, P. Hao, X. Haixian, Y. Ang, X. Meigui, C. Qingli, C. Yuming and Z. Xingfu, *Solid State Sci.*, 2012, **14**, 616–621.
30 H. Tong, N. Enomoto, M. Inada, Y. Tanaka and J. Hojo, *Mater. Lett.*, 2015, **141**, 259–262.
31 J. Archana, M. Navaneethan and Y. Hayakawa, *J. Power Sources*, 2013, **242**, 803–810.
32 E. A. Barringer and H. K. Bowen, *Langmuir*, 1985, **1**, 414–420.
33 S. H. Kang, S. H. Choi, M. S. Kang, J. Y. Kim, H. S. Kim, T. Hyeon and Y. E. Sung, *Adv. Mater.*, 2008, **20**, 54–58.
34 T. Ohsaka, *J. Phys. Soc. Jpn.*, 1980, **48**, 1661–1668.
35 B. Karunagaran, K. Kim, D. Mangalraj, J. Yi and S. Velumani, *Sol. Energy Mater. Sol. Cells*, 2005, **88**, 199–208.
36 Y. Li, Y. Duan and W. Li, *Spectrosc. Spectral Anal.*, 2000, **20**, 699–701.

37 C. Hyun Chul, J. Young Mee and K. Seung Bin, *Vib. Spectrosc.*, 2005, **37**, 33–38.
38 P. Cheng, P. Sun, S. Du, Y. Cai, X. Li, Z. Wang, F. Liu, J. Zheng and G. Lu, *RSC Adv.*, 2014, **4**, 23396–23404.
39 R. G. Satyanarayanan, Y. Chrisopher and B. Palani, *J. Mater. Chem.*, 2012, **22**, 10873–10882.
40 Z. Yan-Zhen, D. Haiyang, L. Yu, T. Xia, C. Guozhong and C. Jian-Feng, *J. Power Sources*, 2014, **254**, 153–160.
41 Z. Yang, C. Y. Chen, C. W. Liu and H. T. Chang, *Adv. Energy Mater.*, 2011, **1**, 259–264.
42 S. F. Shaikh, R. S. Mane and O. S. Joo, *RSC Adv.*, 2014, **4**, 35919–35927.
43 H. J. Snaith and C. Ducati, *Nano Lett.*, 2010, **10**, 1259–1265.